

## Logic Gates Based on Synthetic Antiferromagnetic Bilayer Skyrmions


Mouad Fattouhi<sup>1,\*</sup>, Kai Yu Mak<sup>2,†</sup>, Yan Zhou<sup>2</sup>, Xichao Zhang<sup>3</sup>, Xiaoxi Liu<sup>3</sup>, and Mohamed El Hafidi<sup>4</sup>

<sup>1</sup>*Department of Applied Physics, University of Salamanca, 37008 Salamanca, Spain*

<sup>2</sup>*School of Science and Engineering, the Chinese University of Hong Kong, Shenzhen, Guangdong 518172, China*

<sup>3</sup>*Department of Electrical and Computer Engineering, Shinshu University, 4-17-1 Wakasato, Nagano 380-8553, Japan*

<sup>4</sup>*Condensed Matter Physics Laboratory, Hassan II University of Casablanca, Faculty of Sciences Ben M'Sik, 7955 Casablanca, Morocco*

 (Received 18 January 2021; revised 20 May 2021; accepted 21 June 2021; published 15 July 2021)

Technologies based on magnetic skyrmions, such as computational devices that can operate at high speed or with low energy consumption, have been proposed by many researchers. Recently, synthetic antiferromagnetic (SAF) structures have been proposed to increase the stability and mobility of skyrmions by reducing or eliminating the skyrmion Hall effect. Here, we numerically study the current-induced dynamics of skyrmions on SAF bilayer structures. We demonstrate the effective control and manipulation of SAF skyrmions, including directional displacement and alignment. Furthermore, we design SAF-skyrmion-based logic gates, such as the AND, OR, XOR, and NOT gates. Our design provides guidance for future development of spintronic computing devices that use topological nanoscale spin textures as information carriers.

DOI: [10.1103/PhysRevApplied.16.014040](https://doi.org/10.1103/PhysRevApplied.16.014040)

### I. INTRODUCTION

The magnetic skyrmion is one of the most useful magnetic spin textures that shows nontrivial topology. The existence of skyrmions in magnets was predicted by Bogdanov *et al.* in 1989 [1] and magnetic skyrmions were observed experimentally for the first time in 2009 [2]. By virtue of their high potential in future spintronic applications, magnetic skyrmions have aroused a particular interest in the spintronics community [3–9]. A number of theoretical and experimental works have shown that skyrmions can exist in different types of ferromagnetic (FM) systems, including bulk materials [10–12], thin films [13–15], and multilayers [16–23].

The promising feature of magnetic skyrmions is they can be used to build the next generation of information storage and logic computing devices [24–26]. Nanoscale skyrmions carrying binary information can be displaced in thin films and nanotracks driven by a moderate electric current [27], which is an effective way for transmitting information [28]. For example, the magnetic skyrmion-based racetrack memory is an advanced information storage

device [29] based on the conventional domain-wall-based racetrack memory [30], where magnetic skyrmions move in FM nanotracks driven by a spin-polarized current. However, several obstacles, such as the skyrmion Hall effect (SHE), are encountered on the way to making skyrmion-based in-line motion devices reliable and practically commercialized [31–33]. For example, the SHE may result in the unwanted destruction of skyrmions at the edges of the skyrmion-based racetrack memory structure [34]. Therefore, great efforts are deployed to solve problems related to the realization of skyrmion-based devices [35], leading to more complex and prospective designs, such as the racetrack memory based on synthetic antiferromagnetic (SAF) skyrmions [36–38]. Another appealing nonvolatile information storage device is the skyrmion-based magnetic random-access memory [39,40], which is mainly based on the manipulation of magnetic skyrmions in spin-valve structures [41,42]. Since the first experimental observation of skyrmions, the field has also focused on skyrmion-based conventional logic computing devices [43–45] and novel computing strategies [46,47].

In this work, we computationally demonstrate skyrmion-based logic computing by utilizing the current-driven skyrmion motion and skyrmion-skyrmion interactions in a SAF bilayer structure. The studied system is a ferromagnet/spacer/ferromagnet trilayer, where the two FM layers are strictly exchange coupled in an antiferromagnetic

\*mfa@usal.es

†These authors contributed equally to this work.

(AFM) configuration [48]. In such a SAF structure, the SHE of a bilayer skyrmion can be totally suppressed [35].

## II. SIMULATION

### A. Simulation methods

We simulate the SAF skyrmion-based logic computing operations by using the open-source micromagnetic simulator MUMAX3 [49], where the magnetization dynamics are controlled by the Landau-Lifshitz-Gilbert (LLG) equation augmented with spin-orbit torques (SOTs) or spin-transfer torques (STT) [50].

For the skyrmion dynamics driven by SOTs, we consider a current-perpendicular-to-plane (CPP) geometry, and the LLG equation with the dampinglike SOT term to read [51,52]

$$\frac{d\mathbf{m}}{dt} = -\gamma \mathbf{m} \times \mathbf{H}_{\text{eff}} + \alpha \left( \mathbf{m} \times \frac{d\mathbf{m}}{dt} \right) - \frac{\hbar \theta_{\text{SH}} J_{\text{HM}}}{2\mu_0 e M_s t_{\text{FM}}} \mathbf{m} \times (\mathbf{m} \times \boldsymbol{\sigma}) \quad (1)$$

where  $\mathbf{m} = (\mathbf{M}/M_s)$  is the normalized magnetization,  $\gamma$  denotes the gyromagnetic ratio,  $\alpha$  is the Gilbert damping,  $\theta_{\text{SH}}$  is the Spin Hall angle,  $J_{\text{HM}}$  denotes charge current flowing in the heavy metal,  $\mu_0$  is the vacuum permeability,  $e$  is the elementary electron charge,  $M_s$  is the saturation

magnetization,  $t_{\text{FM}}$  is the ferromagnetic layer thickness, and  $\boldsymbol{\sigma} = \vec{u}_y$ , the unit vector along the transversal direction, in our model. The effective field is the functional derivative of the system functional energy

$$\mathbf{H}_{\text{eff}} = -\frac{1}{\mu_0 M_s} \frac{\delta E_{\text{tot}}}{\delta \mathbf{m}}. \quad (2)$$

In this work, the total average energy density  $E_{\text{tot}}$  includes both intra- and interlayer exchange couplings, Dzyaloshinskii-Moriya interaction (DMI), perpendicular magnetic anisotropy (PMA), and demagnetization terms (see Supplemental Material for further information about the theoretical framework [53] and also Refs. [54–56]). The material parameters are given as those of Co/Pt systems with spin Hall angle  $-0.33^\circ$ , exchange stiffness  $A_{\text{intra}} = 15 \text{ pJ m}^{-1}$ , interlayer exchange coupling constant  $J_{\text{inter}} = -6 \text{ mJ/m}^2$ , Gilbert damping coefficient  $\alpha = 0.3$ , saturation magnetization  $M_s = 580 \text{ kA m}^{-1}$ , PMA constant  $K = 0.8 \text{ MJ m}^{-3}$ , and interfacial DMI strength  $D = 3.5 \text{ mJ m}^{-2}$ . To balance the accuracy and efficiency, all models are discretized into tetragonal elements of size  $2 \text{ nm} \times 2 \text{ nm} \times 2 \text{ nm}$ . The effect of the DMI on the structure's total energy and skyrmion size is discussed in Supplemental Material Fig. S1 [53].

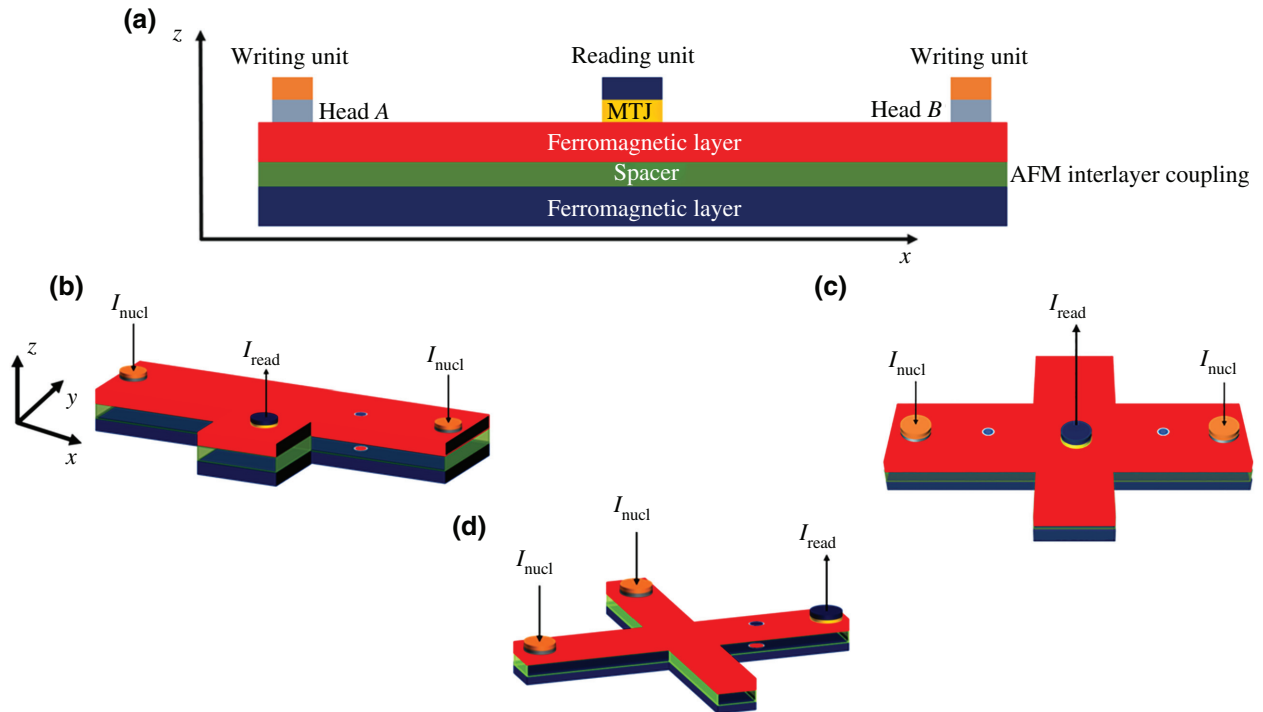


FIG. 1. Schematic illustrations of our simulated SAF structures with a length of 500 nm and a width of 100 nm. The thickness of each FM layer is fixed at 2 nm. (a)  $z$ - $x$  cross section of SAF bilayer used for OR logic gate; (b) OR/AND logic gate schematization; (c) XOR logic gate schematization; (d) NOT logic gate schematization.  $I_{\text{nucl}}$  denotes the skyrmion writing current and  $I_{\text{read}}$  denotes the reading current. MTJ denotes the magnetic tunnel junction for reading the skyrmion at the output.

**B. Design of SAF bilayer structures**

As illustrated in Fig. 1(a), the simulated model is composed of two FM layers separated by a metallic spacer in order to guarantee the existence of an AFM interlayer exchange coupling, which plays a key role in suppressing the SHE.

In this work, skyrmions are driven using SOTs. The charge current is injected into the heavy metal substrate and the spin current is present in the bottom FM layer [57]. The interlayer exchange coupling in this situation drives the skyrmion in the top FM layer. The electric current distributions in the heavy metal are simulated using COMSOL Multiphysics [58], and the profiles found are applied in the micromagnetic simulation to examine the reliability of our designed logic gates. The experimental realization of our logic gates is discussed in Sec. IV B.

**III. SKYRMION DYNAMICS ON SAF BILAYER STRUCTURES**

We first study the skyrmion dynamics on SAF bilayer structures when the out-of-plane current is applied. It is known that different current characteristics can serve to induce skyrmion dynamics. The two methods widely used are the STT, consisting of a current flowing inside the FM layer, and the SOT, which is based on a current flowing in a heavy metal substrate. Recently, several skyrmion dynamics studies have found discrepancies between experimental and analytical results based on the Thiele model, where the interfacial STT has a significant effect on the ultrathin structure with small skyrmions [59,60]. The combination of the interfacial STT and the SOT results in smaller skyrmion Hall angles in experiment. However, in the SAF structure, the SHE is exactly cancelled due to the coupling between skyrmions on the top FM layer and the bottom FM layer. Therefore, the interfacial STT is not considered in this work.

In our study, we use the SOT driving method to move magnetic skyrmions in the SAF structure. Different current densities are applied to induce the SOT to drive the skyrmions at both ends toward the center, as shown in Fig. 2. At a driving current density of  $50 \text{ MA cm}^{-2}$ ,

skyrmions move toward the center and stabilize at 4.5 ns. To understand the trajectory of the skyrmions, we consider forces that contribute to their motion and pinning. Previous studies reported several important forces that are present when skyrmions are moving on nanotracks [27,61], including skyrmion-skyrmion repulsion, the Magnus forces (related to the SHE), the skyrmion-edge repulsion, and the driving force. For our SAF structure, only the skyrmion-skyrmion repulsion, Skyrmion-edge repulsion, and the driving force resulting from the SOT are considered.

The stabilization of the skyrmions at the center when we apply a current density of  $50 \text{ MA cm}^{-2}$  can be understood as the interplay between the driving force and the repulsion force between skyrmions after they collide with each other. In this situation, the driving force is not strong enough to surpass the skyrmion-skyrmion repulsion and causes skyrmions to get closer.

The speed of the skyrmions increases and the spacing between skyrmions decreases as we enhance the current density applied on the structure. The increase in current density induces a greater driving force, hence reducing spacing between skyrmions. The spacing between two skyrmions after collision (at the simulation end when the skyrmion pair is reaching an equilibrium under compensating driving forces) with respect to the applied current density is shown in Fig. 3. In the first portion of the curve, the spacing between two skyrmions decreases as the applied current density increases. It reaches a minimum when the current density equals  $100 \text{ MA cm}^{-2}$ .

When the applied current density is larger than  $100 \text{ MA cm}^{-2}$ , a further increase in current density increases the spacing between skyrmions until the current density reaches  $200 \text{ MA cm}^{-2}$ , as demonstrated in Fig. 3. This increase in spacing can be related to the skyrmion size and the trajectory changes, as shown in Fig. 2 and the inset b of Fig. 3. It is noticed that the skyrmion size reduces as the current density increases, which may be due to the action of the compression force contributed by the driving force and skyrmion-skyrmion repulsion. In addition, we can see the motion changes as the skyrmions reach the center. Instead of stabilizing in the

$J_{\text{HM}}(\text{MA cm}^{-2})$	50	200	500
SOT Skyrmion motion	0 ns	0 ns	0 ns
	2 ns	0.75 ns	0.5 ns
	4.5 ns	4 ns	1.2 ns

FIG. 2. Dynamics of skyrmions in a SAF bilayer nanotrack driven by the SOT at different current densities. The spin current is injected into the bottom FM layer coming from the heavy metal substrate.

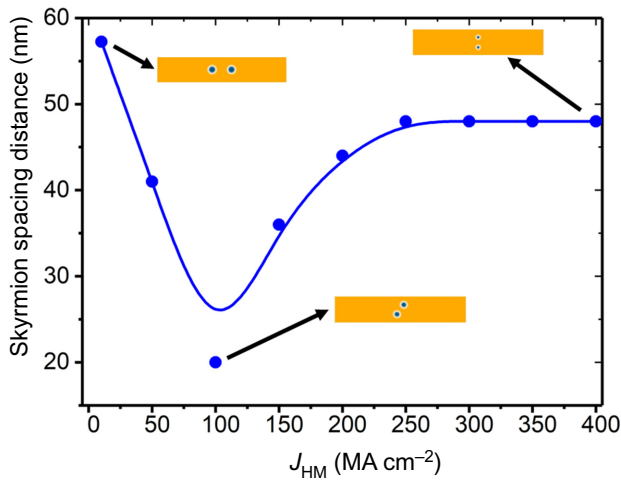


FIG. 3. Spacing between two skyrmions in the final state as a function of the current density applied to the system. Current density is applied ranging from 10 to 400 MA cm<sup>-2</sup>. The spacing is measured once the skyrmions have stabilized after collision.

same horizon, both skyrmions start moving in the vertical direction. This movement is seen after the skyrmions shrink in size, which gives the skyrmions additional space and directions to move in on the narrow nanotrack. As a result, an angle between the driving force and the skyrmion-skyrmion repulsion force is created. Thus, the vertical component of the skyrmion-skyrmion repulsion force repels the skyrmions vertically, creating more space between them. The increase in spacing stops when the skyrmions are aligned vertically in the center.

Further increases in current density cause the skyrmion pair to rotate through an angle of 90° and align vertically at the center, as shown in the third column of Fig. 2 (500 MA cm<sup>-2</sup>). The result is consistent with Fig. 3, where the distances between skyrmions barely change

with respect to the increase of current density beyond 200 MA cm<sup>-2</sup>. These trajectory changes show that the driving force induced by the current density is competing with the repulsive force between the two skyrmions.

Based on these studied dynamic properties of skyrmions, we successfully induce motion and alignment of skyrmions on SAF bilayer structures. Thus, with these basic operations, we are able to design efficient elementary logic gates, including the AND, OR, XOR, and NOT gates. Recently, many devices based on skyrmions have been proposed [62,63]. It is believed that skyrmion-based computing devices are promising as they have the advantages of low energy consumption and can operate at extreme high speed [64–71]. The design of logic gates proposed in this work is summarized in Fig. 1.

#### IV. SAF SKYRMION-BASED LOGIC GATES

##### A. Proof of concept

###### 1. OR logic gate

The logical OR gate is constructed on three-terminal SAF bilayer structures as illustrated in Fig. 1(b). Input *A* and input *B* are located at the left and the right ends of the structure. The output is located in the center of the structure. In skyrmionic logic, the presence of a skyrmion represents logical 1 and the FM ground state represents logical 0. The logical OR gate is operated such that 0 + 0 = 0, 1 + 0 = 1, 0 + 1 = 1 and 1 + 1 = 1. We demonstrate the operation of the OR gate in Fig. 4. The process of 0 + 0 = 0 is trivial, meaning that there is no skyrmion on the input and the output. The process of 1 + 0 = 1 is interpreted as follows. When a skyrmion is present in input *A* and no skyrmion in input *B*, only one skyrmion will travel to the output, representing logical 1 (Fig. 4, left panel). Similarly, the process 0 + 1 = 1 is interpreted by the presence of a skyrmion in input *B* and the absence of a skyrmion in

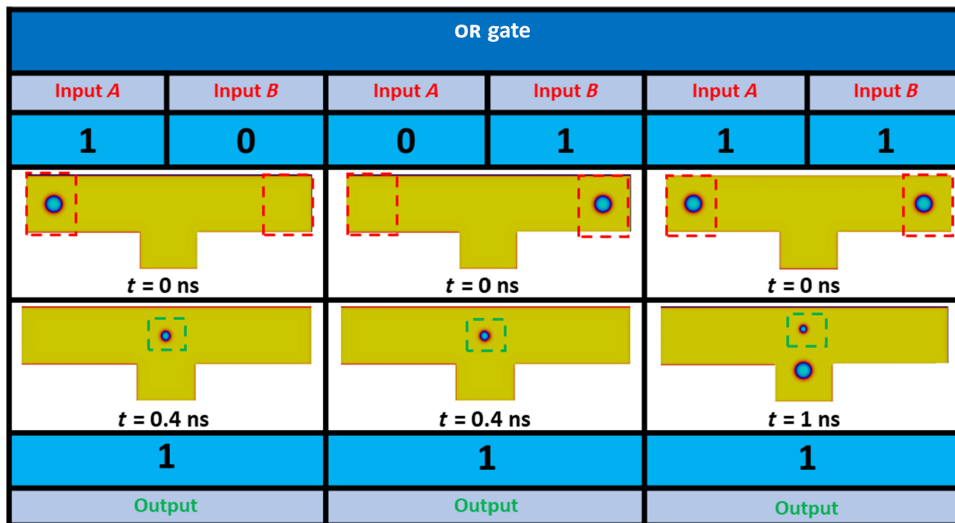


FIG. 4. Logical OR operation based on SAF bilayer skyrmions. The skyrmion represents logical 1 and the FM ground state represents logical 0. The logical OR gate is constructed on three-terminal SAF bilayer structures with a 500 MA cm<sup>-2</sup> working current. The input *A* and input *B* (red square) are two ends of the SAF bilayer structures while the output detection is made in the central area (green square).

input  $A$ . The skyrmion travels to the center, representing logical 1 in the output (Fig. 4, middle panel). The most important process  $1 + 1 = 1$  is interpreted by the presence of skyrmions in both input  $A$  and input  $B$ . Two skyrmions align themselves vertically in the center (Fig. 4, right panel). The repulsion force interacts between the vertically aligned skyrmions, and pushes one of them into the protruding area, which represents logical 1 in the output.

### 2. AND logic gate

The SAF bilayer AND logic gate is designed with a structure similar to that of the OR gate. It differs from the OR gate in that the detection area (output) is on the protruding area next to the center of the SAF structure as shown in Fig. 1(b). In skyrmionic logic, the presence of a skyrmion represents logical 1 and the FM ground state represents logical 0. The logical AND gate is operated such that  $0 + 0 = 0$ ,  $1 + 0 = 0$ ,  $0 + 1 = 0$ , and  $1 + 1 = 1$ . During operation, out-of-plane currents applied on both sides induce the SOT to push the skyrmion toward the center. We demonstrate the operation of the AND gate in Fig. 5. The process of  $0 + 0 = 0$  is trivial, meaning that there is no skyrmion in the input or output. The processes of  $1 + 0 = 0$  and  $0 + 1 = 0$  are similar to those for the OR gate, where a skyrmion is present at either input  $A$  or input  $B$  to represent logical 1, and the ground state on the other input represents logical 0. However, since the output is no longer at the center, the skyrmion stabilized in the center will not enter the protruding area next to it. Thus, no skyrmion can reach the output, representing logical 0 (Fig. 5, left and middle panels). The most important operation  $1 + 1 = 1$  is interpreted by the presence of skyrmions at both input  $A$  and input  $B$ . Two skyrmions will meet each other and align themselves vertically in the center. The repulsion force interacts between the vertically aligned skyrmions, and pushes one

of them into the protruding area, which represents logical 1 in the output (Fig. 5, right panel).

### 3. XOR logic gate

The SAF bilayer XOR logic gate is designed with a structure similar to that of the OR gate. It differs from the OR gate in that the detection area (output) is at the center of the track, with two protruding areas next to it, as shown in Fig. 1(c). In skyrmionic logic, the presence of a skyrmion denotes logical 1 and the FM ground state represents logical 0. The logical XOR gate is operated such that  $0 + 0 = 0$ ,  $1 + 0 = 1$ ,  $0 + 1 = 1$ , and  $1 + 1 = 0$ . During operation, out-of-plane currents are applied on both sides, inducing a SOT force to push the skyrmion toward the center. We demonstrate the operation of the XOR gate in Fig. 6. As with the OR gate, the process of  $0 + 0 = 0$  is trivial, meaning that there is no skyrmion at the input or the output. The processes of  $1 + 0 = 1$  and  $0 + 1 = 1$  are similar to those for the OR gate, in that a skyrmion is present at either input  $A$  or input  $B$  to symbolize logical 1 and the ground state at the other input signifies logical 0. The skyrmions will stabilize in the output area located in the center, representing the output logical 1 (Fig. 6, left and middle panels). The most important operation  $1 + 1 = 0$  is interpreted by the presence of skyrmions at both input  $A$  and input  $B$ . Two skyrmions will meet each other in the center, and due to the repulsive interaction, they will push one another away from the output area in the center. The lack of the skyrmion represents logical 0 in the output (Fig. 6, right panel).

### 4. NOT logic gate

For the NOT logic gate, the concept is different. We try to drive the skyrmion along two crossed nanotracks. The input region is located at the start of each nanotrack and

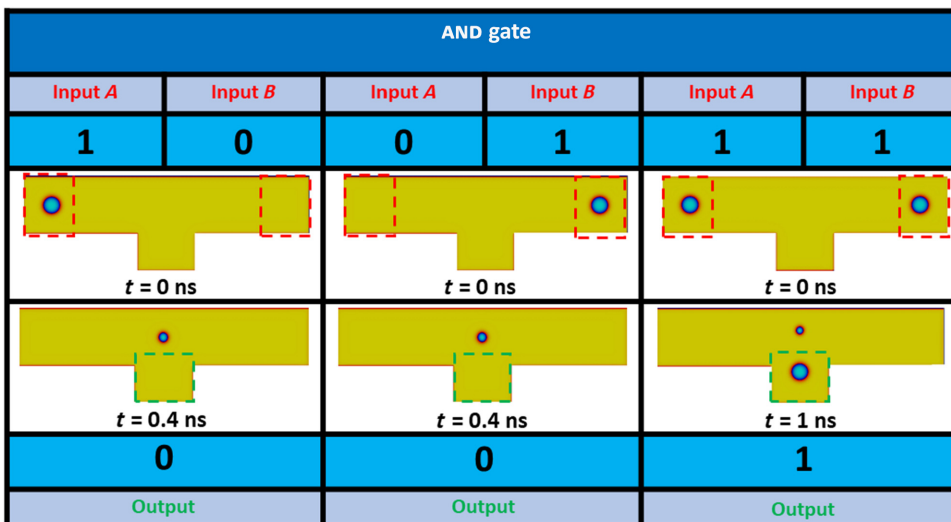


FIG. 5. Logical AND operation based on SAF bilayer skyrmions. The skyrmion represents logical 1 and the FM ground state represents logical 0. The logical AND gate is constructed on three-terminal SAF bilayer structures with a  $500 \text{ MA cm}^{-2}$  working current. The input  $A$  and input  $B$  (red square) are two ends of the SAF bilayer structures while the output is detected in the protruding area in the center (green square).



XOR gate					
Input A	Input B	Input A	Input B	Input A	Input B
1	0	0	1	1	1
1	1	1	1	0	0
Output	Output	Output	Output	Output	Output

FIG. 6. Logical XOR operation based on SAF bilayer skyrmions. The skyrmion represents logical 1 and the FM ground state represent logical 0. The logical XOR gate is constructed on three-terminal SAF bilayer structures with a  $500 \text{ MA cm}^{-2}$  working current as illustrated in Fig. 1(c). The input  $A$  and input  $B$  (red square) are at the two ends of the SAF bilayer structure while the output is detected in the protruding area in the center (green square).

the output is at the end of the second track [see Fig. 1(d)]. The presence of a skyrmion on the first track input region represents logical 1 and the presence of a skyrmion on the second track input region represents logical 0. For the NOT gate operation, we have  $1 = 0$  and  $0 = 1$ . As shown in Fig. 7, the case  $1 = 0$  is interpreted by placing a skyrmion in the input region on the first nanotrack. An out-of-plane current is applied to drive the skyrmion toward the end. The absence of a skyrmion in the output region of the first nanotrack and its presence in the output region of the second nanotrack represents logical 0 in the output (Fig. 7, left panel). The case  $0 = 1$  is interpreted by placing a skyrmion in the input region on the second nanotrack. An out-of-plane current is applied to drive the skyrmion toward the end. The presence of skyrmion in the output region of the first nanotrack and its absence in the output region of the second nanotrack represents logical 1 in the output (Fig. 7, right panel).

### B. Logic gates with realistic current values

Now we study the feasibility of realizing the proposed skyrmion logic gates based on SAFs. In our design, the skyrmion logic computation is executed by controlling the skyrmion trajectory, which is induced by the electric currents flowing toward the center. Therefore, the grounding of the system may alter the electric current when the grounding contact is small. We investigate this issue with electric current simulation using the electrical module of COMSOL Multiphysics [58], where different grounding sizes are applied to understand their effect on current distribution in the heavy metal substrate, as shown in Fig. 8. Since our micromagnetic simulations are carried out using Co/Pt multilayer parameters, we simulate in COMSOL a Pt layer with an electrical conductivity  $\sigma = 9.43 \times 10^6 \text{ S m}^{-1}$ , a resistivity of  $\rho = 1.06 \times 10^{-7} \Omega \text{ m}^{-1}$ , and relative permittivity  $\epsilon_1 = 0.7347$ ,  $\epsilon_2 = 2.7604$ . These

current distribution profiles are applied to the micromagnetic simulation, where we find that the logical computation of the OR, AND, and XOR gates can be achieved with a grounding size of 40 nm or above.

On the other hand, the previous results are carried out with the material parameters presented in Sec. II. Currently, experiments on Pt/Co multilayer thin films suggests that the Gilbert's damping coefficient in such systems is lower [72–75]. Therefore, recent studies on skyrmion logic gates are usually conducted with  $\alpha = 0.1$  [43,76]. We apply these findings on our design and find that the current density required in our system is greatly reduced to  $50 \text{ MA cm}^{-2}$ .

NOT gate SOT	
Input	Input
1	0
0	1
Output	Output

FIG. 7. Logical NOT operation based on SAF bilayer skyrmions. The logical NOT gate is constructed by a cross-shaped structure made of SAF bilayer tracks with a  $300 \text{ MA cm}^{-2}$  working current as shown in Fig. 1(d).

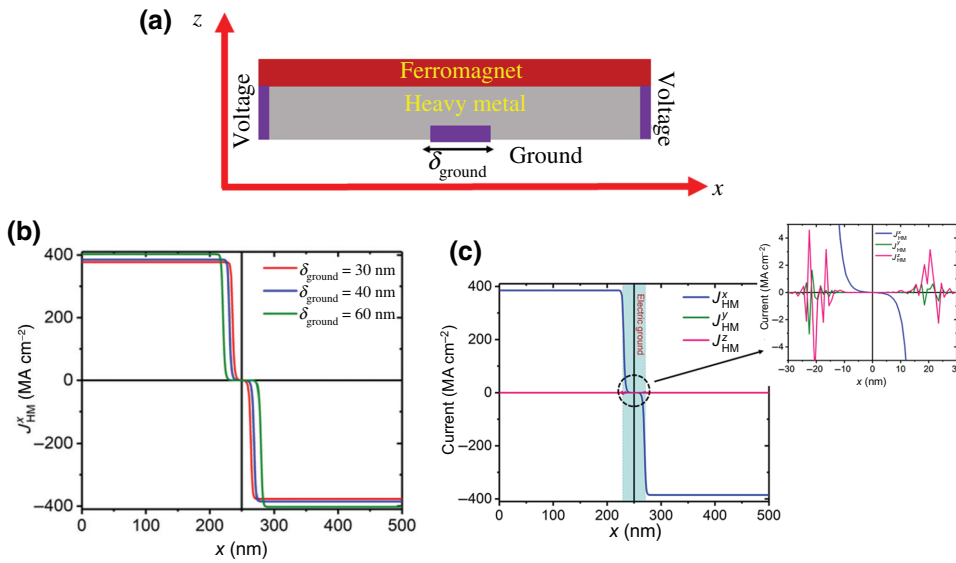
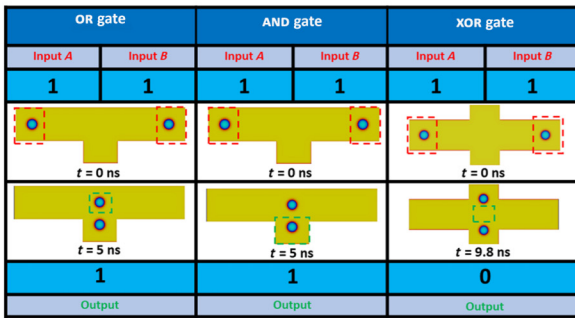


FIG. 8. Current distribution inside a heavy metal (Pt) layer. (a) Sketch of the simulated device; (b) the longitudinal current component along the system length for three different sizes of the electric grounding; (c) the three spatial current components for  $\delta_{\text{ground}} = 40$  nm. The inset shows an enlargement of the grounded part for the three components of the electric current density.

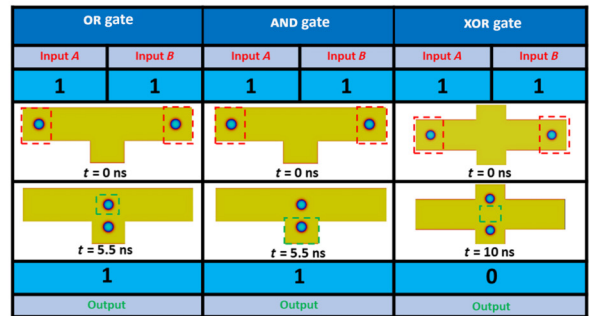
As demonstrated in Figs. 9(a)–9(c), the critical operation 1 + 1 of the three gates is realized by applying a current density of  $50 \text{ MA cm}^{-2}$ , which is lower than the current densities  $100 \text{ MA cm}^{-2}$  or  $300 \text{ MA cm}^{-2}$  used in previous experimental works on SAF structures [77,78]. Furthermore, we also take into consideration the effect of

the electric grounding on the current created on our system by applying the current profiles from COMSOL simulations. As a result, our gates are valid for systems with an electric ground length  $\delta_{\text{ground}} = 40$  nm as shown in Fig. 9(c). Additionally, the required current density for the operation of AND, OR, and NOT gates can be further decreased

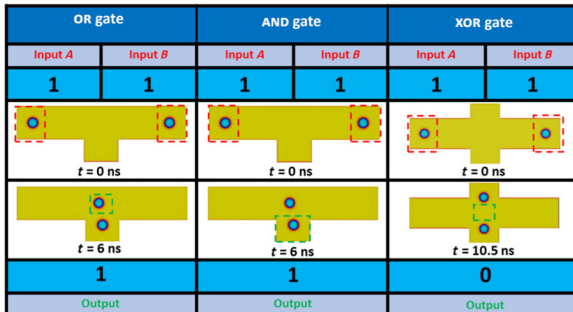
(a)  $J_{\text{HM}} = 50 \text{ MA cm}^{-2}, \delta_{\text{ground}} = 20 \text{ nm}$



(b)  $J_{\text{HM}} = 50 \text{ MA cm}^{-2}, \delta_{\text{ground}} = 30 \text{ nm}$



(c)  $J_{\text{HM}} = 50 \text{ MA cm}^{-2}, \delta_{\text{ground}} = 40 \text{ nm}$



(d)  $J_{\text{HM}} = 30 \text{ MA cm}^{-2}, \text{Co-Fe-B}$

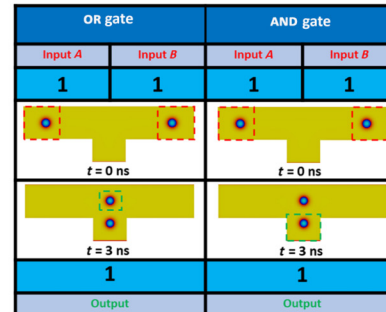


FIG. 9. SAF skyrmion OR, AND, XOR logic gates made with Co/Pt with different electric grounding lengths and Co-Fe-B. (a) Logic gates implemented in Co/Pt with  $\alpha = 0.1$  and  $\delta_{\text{ground}} = 20$  nm; (b) logic gates implemented in Co/Pt with  $\alpha = 0.1$  and  $\delta_{\text{ground}} = 30$  nm; (c) logic gates implemented in Co/Pt with  $\alpha = 0.1$  and  $\delta_{\text{ground}} = 40$  nm; (d) OR, AND logic gates implemented in Co-Fe-B/HM with  $\alpha = 0.015$ . We present in the figure only the 1+1 operations since the 1+0, 0+1 and 0+0 operations are easy to achieve at low current values.

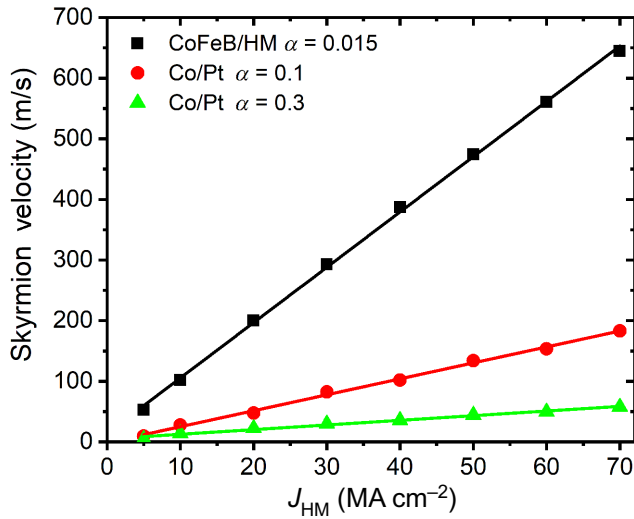


FIG. 10. SAF skyrmion speed versus current for three different systems. The green and red curves show the skyrmion velocity evolution versus current for Co/Pt with the material parameters listed in Sec. II and  $\alpha = 0.3$  and  $\alpha = 0.1$ , respectively. The black curve shows the skyrmion velocity versus current for Co-Fe-B with material parameters as follows:  $A_{\text{intra}} = 20$  pJ m<sup>-1</sup>,  $\alpha = 0.015$ ,  $M_s = 1$  kA m<sup>-1</sup>,  $K_u = 0.8$  MJ m<sup>-3</sup>,  $D = 1.8$  mJ m<sup>-2</sup>, and  $J_{\text{inter}} = -8$  mJ m<sup>-2</sup>.

to 30 MA cm<sup>-2</sup> when these skyrmion-based logic gates are realized on Co-Fe-B, as shown in Fig. 9(d) [28].

Our findings demonstrate that the electric current required to execute logical operations varies in materials with different damping coefficients  $\alpha$ . Thus, we perform micromagnetic simulation analysis to study skyrmion motion on the three systems (Co-Fe-B, Co/Pt with  $\alpha = 0.1$ , and Co/Pt with  $\alpha = 0.3$ ) with different applied electric current densities. It is obvious that the skyrmion velocities are significantly enhanced in Co-Fe-B and Co/Pt with  $\alpha = 0.1$  systems when compared with the skyrmion velocity in Co/Pt with  $\alpha = 0.3$  under the same electric current density. The enhancement of velocity by the reduction in the damping coefficient of the materials can be explained by the skyrmion motion in Thiele’s framework as given by [79]

$$\vec{G}_{\text{sk}} \times \vec{v} + \alpha \overleftrightarrow{D}_{\text{sk}} \vec{v} = \vec{F}_d \quad (3)$$

where  $\vec{v}$  is the skyrmion velocity,  $\vec{G}_{\text{sk}}$  is the gyrovector,  $\overleftrightarrow{D}_{\text{sk}}$  is the dissipation tensor, and  $\vec{F}_d$  is the driving force due to the spin Hall effect. In SAF structures, the gyrovector is reduced to zero, as described by [35], and the dissipation tensor  $\overleftrightarrow{D}_{\text{sk}}$  could be expressed using a  $2 \times 2$  matrix

$$\overleftrightarrow{D}_{\text{sk}} = \begin{pmatrix} D & 0 \\ 0 & D \end{pmatrix}.$$

Therefore, Eq. (3) can be reduced to  $v = (F_d/\alpha D)$ , where the skyrmion velocity is inversely proportional to the damping coefficient  $\alpha$ . As a result, in materials with a lower damping coefficient  $\alpha$ , the same skyrmion motion can be obtained with a lower current density, as demonstrated in Fig. 10.

## V. CONCLUSIONS

Skyrmion-based techniques provide promising routes to fabricate computational devices that can operate at high speed or with low energy consumption. In this work, we analyze the dynamics of skyrmions on SAF bilayer structures at different current densities, where the current is applied in opposite directions. Our results indicate that using an electrical current, the skyrmions interaction, and the skyrmion-edge repulsion we can align and rotate skyrmions in SAF bilayer structures. With these findings, we are able to design elementary logic gates that are essential for skyrmion-based computational devices. Hence, we report the designed and simulated results of OR, NOT, AND, and XOR logic gates that are built on SAF bilayer structures. Our results provide information for designing computational magnetic devices that use topological nanoscale spin textures as information carriers. Moreover, our results will help to design future magnetic devices and spintronic devices.

## ACKNOWLEDGMENTS

M.F. acknowledges the funding from the European Union’s Framework Program for Research and Innovation Horizon 2020 (2014–2020) under the Marie Skłodowska-Curie Grant Agreement No. 860060 (ITN MagnEfi). X.Z. received support from an International Research Fellowship of the Japan Society for the Promotion of Science (JSPS). X.Z. is supported by JSPS KAKENHI (Grant No. JP20F20363). X.L. acknowledges the support by the Grants-in-Aid for Scientific Research from JSPS KAKENHI (Grants No. JP20F20363 and No. JP21H01364). Y.Z. acknowledges the support by the Guangdong Special Support Project (Grant No. 2019BT02X030), Shenzhen Peacock Group Plan (Grant No. KQTD20180413181702403), Pearl River Recruitment Program of Talents (Grant No. 2017GC010293), and National Natural Science Foundation of China (Grants No. 11974298 and No. 61961136006). The authors thank Felipe Garcia-Sanchez, Eduardo Martinez and Rocio Yanes-Diaz for the fruitful discussions. M.F. thanks Luis Lopez-Diaz for providing computation facilities and guidance.

- [1] A. N. Bogdanov and D. A. Yablonskii, Thermodynamically stable “vortices” in magnetically ordered crystals. The mixed state of magnets, *Sov. Phys. JETP* **68**, 101 (1989).



- [2] S. Mühlbauer, B. Binz, F. Jonietz, C. Pfleiderer, A. Rosch, A. Neubauer, R. Georgii, and P. Böni, Skyrmion lattice in a chiral magnet, *Science* **323**, 915 (2009).
- [3] Albert Fert, Nicolas Reyren, and Vincent Cros, Magnetic skyrmions: Advances in physics and potential applications, *Nat Rev. Mater* **2**, 17031 (2017).
- [4] W. Kang, Y. Huang, X. Zhang, Y. Zhou, and W. Zhao, Skyrmion-Electronics: An overview and outlook, *Proc. IEEE* **104**, 2040 (2016).
- [5] Roland Wiesendanger, Nanoscale magnetic skyrmions in metallic films and multilayers: A new twist for spintronics, *Nat Rev. Mat.* **1**, 16044 (2016).
- [6] Niklas Romming, André Kubetzka, Christian Hanneken, Kirsten von Bergmann, and Roland Wiesendanger, Field-dependent Size and Shape of Single Magnetic Skyrmions, *Phys. Rev. Lett.* **114**, 177203 (2015).
- [7] K. Everschor-Sitte, J. Masell, R. M. Reeve, and M. Kläui, Perspective: Magnetic skyrmions—overview of recent progress in an active research field, *J. Appl. Phys.* **124**, 240901 (2018).
- [8] Xiangjun Xing, Philip W. T. Pong, and Yan Zhou, Skyrmion domain wall collision and domain wall-gated skyrmion logic, *Phys. Rev. B.* **94**, 054408 (2016).
- [9] Shanquan Chen, Shuai Yuan, Zhipeng Hou, Yunlong Tang, Jinping Zhang, Tao Wang, Kang Li, Weiwei Zhao, Xingjun Liu, Lang Chen, Lane W. Martin, and Zuhuang Chen, Recent progress on topological structures in ferroic thin films and heterostructures, *Adv. Mat.* **33**, 2000857 (2021).
- [10] A. Chacon, L. Heinen, M. Halder, A. Bauer, W. Simeth, S. Mühlbauer, H. Berger, M. Garst, A. Rosch, and C. Pfleiderer, Real-space observation of skyrmion lattice in helimagnet MnSi thin samples, *Nano Lett.* **12**, 1673 (2012).
- [11] X. Z. Yu, W. Koshibae, Y. Tokunaga, K. Shibata, Y. Taguchi, N. Nagaosa, and Y. Tokura, Transformation between meron and skyrmion topological spin textures in a chiral magnet, *Nature* **564**, 95 (2018).
- [12] X. Z. Yu, D. Morikawa, Y. Tokunaga, M. Kubota, T. Kurumaji, H. Oike, M. Nakamura, F. Kagawa, Y. Taguchi, T.-h. Arima, M. Kawasaki, and Y. Tokura, Current-induced nucleation and annihilation of magnetic skyrmions at room temperature in a chiral magnet, *Adv. Mater.* **29**, 1606178 (2017).
- [13] Mouad Fattouhi, Moulay Youssef El Hafidi, and Mohamed El Hafidi, Formation of a hexagonal skyrmion lattice assisted by magnetic field in CeFeB ultrathin films, *J. Magn. Magn. Mater* **495**, 165870 (2020).
- [14] Sebastian Meyer, Marco Perini, Stephan von Malotki, André Kubetzka, Roland Wiesendanger, Kirsten von Bergmann, and Stefan Heinze, Isolated zero field sub-10 nm skyrmions in ultrathin Co films, *Nat. Comm.* **10**, 3823 (2019).
- [15] Kai Litzius, Jonathan Leliaert, Pedram Bassirian, Davi Rodrigues, Sascha Kromin, Ivan Leshch, Jakub Zazvorka, Kyu-Joon Lee, Jeroen Mulkers, Nico Kerber, Daniel Heinze, Niklas Keil, Robert M. Reeve, Markus Weigand, Bartel Van Waeyenberge, Gisela Schütz, Karin Everschor-Sitte, Geoffrey S. D. Beach, and Mathias Kläui, The role of temperature and drive current in skyrmion dynamics, *Nat. Electron.* **3**, 30 (2020).
- [16] Anjan Soumyanarayanan, M. Raju, A. L. Gonzalez Oyarce, Anthony K. C. Tan, Mi-Young Im, A. P. Petrović, Pin Ho, K. H. Khoo, M. Tran, C. K. Gan, F. Ernult, and C. Panagopoulos, Tunable room-temperature magnetic skyrmions in Ir/Fe/Co/Pt multilayers, *Nat. Mater.* **16**, 898 (2017).
- [17] I. Leshch and G. S. D. Beach, Walker Breakdown with a Twist: Dynamics of Multilayer Domain Walls and Skyrmions Driven by Spin-Orbit Torque, *Phys. Rev. Appl.* **12**, 044031 (2019).
- [18] I. Leshch and G. S. D. Beach, Twisted domain walls and skyrmions in perpendicularly magnetized multilayers, *Phys. Rev. B* **98**, 104402 (2018).
- [19] William Legrand, Nathan Ronceray, Nicolas Reyren, Davide Maccariello, Vincent Cros, and Albert Fert, Modeling the Shape of Axisymmetric Skyrmions in Magnetic Multilayers, *Phys. Rev. Appl.* **10**, 064042 (2018).
- [20] J. Zázvorka, F. Jakobs, D. Heinze, N. Keil, S. Kromin, S. Jaiswal, K. Litzius, G. Jakob, P. Virnau, D. Pinna, K. Everschor-Sitte, L. Rózsa, A. Donges, U. Nowak, and M. Kläui, Thermal skyrmion diffusion used in a reshuffler device, *Nat. Nanotechnol.* **14**, 658 (2019).
- [21] M. Lonsky and A. Hoffmann, Coupled skyrmion breathing modes in synthetic ferri- and antiferromagnets, *Phys. Rev. B* **102**, 104403 (2020).
- [22] S. A. Siddiqui, J. Sklenar, K. Kang, M. J. Gilbert, A. Schleife, N. Mason, and A. Hoffmann, Metallic antiferromagnets, *J. Appl. Phys.* **128**, 040904 (2020).
- [23] Olivier Boulle, *et al.*, Room-temperature chiral magnetic skyrmions in ultrathin magnetic nanostructures, *Nat. Nano.* **11**, 449 (2016).
- [24] Giovanni Finocchio, Felix Büttner, Riccardo Tomasello, Mario Carpentieri, and Mathias Kläui, Magnetic skyrmions: From fundamental to applications, *J. Phys. D Appl. Phys.* **49**, 423001 (2016).
- [25] C. Back, V. Cros, H. Ebert, K. Everschor-Sitte, A. Fert, M. Garst, Tianping Ma, S. Mankovsky, T. L. Monchesky, and M. Mostovoy, The 2020 skyrmionics roadmap, *J. Phys. D Appl. Phys.* **53**, 363001 (2020).
- [26] Albert Fert and Frédéric Nguyen Van Dau, Spintronics, from giant magnetoresistance to magnetic skyrmions and topological insulators, *C. R. Phys.* **20**, 817 (2019).
- [27] J. Sampaio, V. Cros, S. Rohart, A. Thiaville, and A. Fert, Nucleation, stability and current-induced motion of isolated magnetic skyrmions in nanostructures, *Nat. Nanotechnol.* **8**, 839 (2013).
- [28] R. Tomasello, E. Martinez, R. Zivieri, L. Torres, M. Carpentieri, and G. Finocchio, A strategy for the design of skyrmion racetrack memories, *Sci. Rep.* **4**, 6784 (2014).
- [29] Kang Wang, Lijuan Qian, See-Chen Ying, Gang Xiao, and Xiaoshan Wu, Controlled modification of skyrmion information in a three-terminal racetrack memory, *Nanoscale* **11**, 6952 (2019).
- [30] S. Parkin, Masamitsu Hayashi, and Luc Thomas, Magnetic domain-wall racetrack memory, *Science* **320**, 190 (2008).
- [31] G. Chen, Skyrmion Hall effect, *Nat. Phys.* **13**, 112 (2017).
- [32] K. Litzius, I. Leshch, B. Krüger, P. Bassirian, L. Caretta, K. Richter, F. Büttner, K. Sato, O. A. Tretiakov, J. Förster, R. M. Reeve, M. Weigand, I. Bykova, H. Stoll, G. Schütz, G. S. D. Beach, and M. Kläui, Skyrmion Hall effect revealed by direct time-resolved X-ray microscopy, *Nat. Phys.* **13**, 170 (2017).

- [33] C. Reichhardt and C. J. O. Reichhardt, Thermal creep and the skyrmion Hall angle in driven skyrmion crystals, *J. Phys.: Condens. Matter* **31**, 07LT01 (2019).
- [34] Wanjun Jiang, Xichao Zhang, Guoqiang Yu, Wei Zhang, Xiao Wang, M. Benjamin Jungfleisch, John E. Pearson, Xuemei Cheng, Olle Heinonen, Kang L. Wang, Yan Zhou, Axel Hoffmann, and Suzanne G. E. te Velthuis, Direct observation of the skyrmion Hall effect, *Nat. Phys.* **13**, 162 (2017).
- [35] Xichao Zhang, Yan Zhou, and Motohiko Ezawa, Magnetic bilayer-skyrmions without skyrmion Hall effect, *Nat. Comm.* **7**, 10293 (2016).
- [36] Xichao Zhang, Motohiko Ezawa, and Yan Zhou, Thermally stable magnetic skyrmions in multilayer synthetic antiferromagnetic racetracks, *Phys. Rev. B* **94**, 064406 (2016).
- [37] Patrick M. Buhl, Frank Freimuth, Stefan Blügel, and Yuriy Mokrousov, Topological spin Hall effect in antiferromagnetic skyrmions, *P.S.S: Rapid Res. Lett.* **11**, 1700007 (2017).
- [38] R. A. Duine, Kyung-Jin Lee, Stuart S. P. Parkin, and M. D. Stiles, Synthetic antiferromagnetic spintronics, *Nat. Phys.* **14**, 217 (2018).
- [39] X. Chen, H. Zhang, E. Deng, M. Yang, N. Lei, Y. Zhang, W. Kang, and W. Zhao, Sky-RAM: Skyrmionic random access memory, *IEEE Electron Device Lett.* **40**, 722 (2019).
- [40] Sabpreet Bhatti, Rachid Sbiaa, Atsufumi Hirohata, Hideo Ohno, Shunsuke Fukami, and S. N. Piramanayagam, Spintronics based random access memory: A review, *Mater. Today* **20**, 530 (2017).
- [41] J. H. Guo, J. Xia, X. C. Zhang, Philip. W.T. Pong, Y. M. Wu, H. Chen, W. S. Zhao, and Y. Zhou, A ferromagnetic skyrmion-based nano-oscillator with modified profile of Dzyaloshinskii-Moriya interaction, *J. Magn. Magn. Mater* **496**, 165912 (2020).
- [42] Xueying Zhang, Wenlong Cai, Xichao Zhang, Zilu Wang, Zhi Li, Yu Zhang, Kaihua Cao, Na Lei, Wang Kang, Yue Zhang, Haiming Yu, Yan Zhou, and Weisheng Zhao, Skyrmions in magnetic tunnel junctions, *ACS Appl. Mater. Interfaces* **10**, 16887 (2018).
- [43] Maverick Chauwin, Xuan Hu, Felipe Garcia-Sanchez, Neilesh Betrabet, Alexandru Paler, Christoforos Moutafis, and Joseph S. Friedman, Skyrmion Logic System for Large-Scale Reversible Computation, *Phys. Rev. Appl.* **12**, 064053 (2019).
- [44] Shijiang Luo, Min Song, Xin Li, Yue Zhang, Jeongmin Hong, Xiaofei Yang, Xuecheng Zou, Nuo Xu, and Long You, Reconfigurable skyrmion logic gates, *Nano Lett.* **18**, 1180 (2018).
- [45] Xichao Zhang, Motohiko Ezawa, and Yan Zhou, Magnetic skyrmion logic gates: Conversion, duplication and merging of skyrmions, *Sci. Rep.* **5**, 9400 (2015).
- [46] Kyung Mee Song, Jae-Seung Jeong, Biao Pan, Xichao Zhang, Jing Xia, Sunkyung Cha, Tae-Eon Park, Kwangsu Kim, Simone Finizio, Jörg Raabe, Joonyeon Chang, Yan Zhou, Weisheng Zhao, Wang Kang, Hyunsu Ju, and Seonghoon Woo, Skyrmion-based artificial synapses for neuromorphic computing, *Nat. Electron.* **3**, 148 (2020).
- [47] Diana Prychynenko, Matthias Sitte, Kai Litzius, Benjamin Krüger, George Bourianoff, Mathias Kläui, Jairo Sinova, and Karin Everschor-Sitte, Magnetic Skyrmion as a Nonlinear Resistive Element: A Potential Building Block for Reservoir Computing, *Phys. Rev. Appl.* **9**, 014034 (2018).
- [48] Davide Maccariello, William Legrand, Nicolas Reyren, Fernando Ajejas, Karim Bouzehouane, Sophie Collin, Jean-Marie George, Vincent Cros, and Albert Fert, Electrical Signature of Noncollinear Magnetic Textures in Synthetic Antiferromagnets, *Phys. Rev. Appl.* **14**, 051001(R) (2020).
- [49] Arne Vansteenkiste, Jonathan Leliaert, Mykola Dvornik, Mathias Helsen, Felipe Garcia-Sanchez, and Bartel Van Waeyenberge, The design and verification of MuMax3, *AIP Adv.* **4**, 107133 (2014).
- [50] M. Lakshmanan, The fascinating world of the Landau–Lifshitz–Gilbert equation: An overview, *Phil. Trans. R. Soc. A* **369**, 1280 (2011).
- [51] Eduardo Martinez, Satoru Emori, Noel Perez, Luis Torres, and Geoffrey S. D. Beach, Current-driven dynamics of Dzyaloshinskii domain walls in the presence of in-plane fields: Full micromagnetic and one-dimensional analysis, *J. Appl. Phys.* **115**, 213909 (2014).
- [52] J. C. Slonczewski, Current-driven excitation of magnetic multilayers, *J. Magn. Magn. Mater.* **159**, L1 (1996).
- [53] See Supplemental Material <http://link.aps.org/supplemental/10.1103/PhysRevApplied.16.014040>, for further information regarding skyrmions’ static properties and theoretical formulation.
- [54] A. Siemens, Y. Zhang, J. Hagemester, E. Y. Vedmedenko, and R. Wiesendanger, Minimal radius of magnetic skyrmions: Statics and dynamics, *New J. Phys.* **18**, 045021 (2016).
- [55] S. Zhang and Z. Li, Roles of Nonequilibrium Conduction Electrons on the Magnetization Dynamics of Ferromagnets, *Phys. Rev. Lett.* **93**, 127204 (2004).
- [56] N. J. Kim, S. P. Kang, C. Lee, H. G. Yoon, H. Y. Kwon, and C. Won, Versatile motion control of a magnetic skyrmion pair with spin transfer torques, *J. Korean Phys. Soc.* **77**, 10 (2020).
- [57] Seonghoon Woo, Kyung Mee Song, Hee-Sung Han, Min-Seung Jung, Mi-Young Im, Ki-Suk Lee, Kun Soo Song, Peter Fischer, Jung-Il Hong, Jun Woo Choi, Byoung-Chul Min, Hyun Cheol Koo, and Joonyeon Chang, Spin-orbit torque-driven skyrmion dynamics revealed by time-resolved X-ray microscopy, *Nat. Comm.* **8**, 15573 (2017).
- [58] Comsol Multiphysics user’s guide (4.3 ed), COMSOL Multiphysics AB (2012).
- [59] Serban Lepadatu, Effect of inter-layer spin diffusion on skyrmion motion in magnetic multilayers, *Sci. Rep.* **9**, 9592 (2019).
- [60] Callum Robert MacKinnon, Serban Lepadatu, Tim Mercer, and Philip Raymond Bissell, Role of an additional interfacial spin-transfer torque for current-driven skyrmion dynamics in chiral magnetic layers, *Phys. Rev. B* **102**, 214408 (2020).
- [61] Seonghoon Woo, Kai Litzius, Benjamin Krüger, Mi-Young Im, Lucas Caretta, Kornel Richter, Maxwell Mann, Andrea Krone, Robert M. Reeve, Markus Weigand, Parnika Agrawal, Ivan Lemesh, Mohamad-Assaad Mawass, Peter

- Fischer, Mathias Kläui, and Geoffrey S. D. Beach, Observation of room-temperature magnetic skyrmions and their current-driven dynamics in ultrathin metallic ferromagnets, *Nat. Mat.* **15**, 501 (2016).
- [62] Ziyang Yu, Maokang Shen, Zhongming Zeng, Shiheng Liang, Yong Liu, Ming Chen, Zhenhua Zhang, Zhihong Lu, Long You, Xiaofei Yang, Yue Zhang, and Rui Xiong, Voltage-controlled skyrmion-based nanodevices for neuromorphic computing using a synthetic antiferromagnet, *Nanoscale* **2**, 1309 (2020).
- [63] R. Mishra and H. Yang, Emerging spintronics phenomena and applications, *IEEE Trans. Magn* **57**, 0800134 (2021).
- [64] Sai Lia, Wang Kang, Xichao Zhang, Tianxiao Niea, Yan Zhou, Kang L. Wangd, and Weisheng Zhao, Magnetic skyrmions for unconventional computing, *Mater. Horizons* **8**, 854 (2021).
- [65] Marine Schott, Anne Bernand-Mantel, Laurent Ranno, Stefania Pizzini, Jan Vogel, Helene Bea, Claire Baraduc, Stephane Auffret, Gilles Gaudin, and Dominique Givord, The skyrmion switch: Turning magnetic skyrmion bubbles on and off with an electric field, *Nano Lett.* **17**, 3006 (2017).
- [66] Yizheng Liu, Na Lei, Chengxiang Wang, Xichao Zhang, Wang Kang, Daoqian Zhu, Yan Zhou, Xiaoxi Liu, Youguang Zhang, and Weisheng Zhao, Voltage-Driven High-Speed Skyrmion Motion in a Skyrmion-Shift Device, *Phys. Rev. Appl.* **11**, 014004 (2019).
- [67] Xichao Zhang, Yan Zhou, Kyung Mee Song, Tae-Eon Park, Jing Xia, Motohiko Ezawa, Xiaoxi Liu, Weisheng Zhao, Guoping Zhao, and Seonghoon Woo, Skyrmion-electronics: Writing, deleting, reading and processing magnetic skyrmions toward spintronic applications, *J. Phys. Cond. Matt.* **32**, 143001 (2020).
- [68] Zhizhong Zhang, Yuanzhi Zhu, Yue Zhang, Kun Zhang, Jiang Nan, Zhenyi Zheng, Youguang Zhang, and Weisheng Zhao, Skyrmion-based ultra-low power electric-field-controlled reconfigurable (SUPER) logic gate, *IEEE Trans. Electron Devices* **40**, 1984 (2019).
- [69] D. Pinna, G. Bourianoff, and K. Everschor-Sitte, Reservoir Computing with Random Skyrmion Textures, *Phys. Rev. Appl.* **14**, 054020 (2020).
- [70] Meghna G. Mankalale, Zhengyang Zhao, Jian-Ping Wang, and Sachin S. Sapatnekar, Skylogic—A proposal for a skyrmion-based logic device, *IEEE Trans. Electron Devices* **66**, 1990 (2019).
- [71] R. Tomasello, V. Puliafito, E. Martinez, A. Manchon, M. Ricci, M. Carpentieri, and G. Finocchio, Performance of synthetic antiferromagnetic racetrack memory: Domain wall versus skyrmion, *J. Phys. D: Appl. Phys.* **50**, 325302 (2017).
- [72] Thibaut Devolder, S. Couet, J. Swerts, and G. S. Kar, Gilbert damping of high anisotropy Co/Pt multilayers, *J. Phys. D: Appl. Phys.* **51**, 135002 (2018).
- [73] P. Neilinger, T. Štěpka, M. Mruczkiewicz, J. Dérer, D. Mancaa, E. Dobročka, A. S. Samardakd, M. Grajcar, and V. Cambel, Ferromagnetic resonance study of sputtered Pt/Co/Pt multilayers, *Appl. Surf. Sci.* **461**, 202 (2020).
- [74] T. Devolder, Joo-Von Kim, F. Garcia-Sanchez, J. Swerts, W. Kim, S. Couet, G. Kar, and A. Furnemont, Time-resolved spin-torque switching in MgO-based perpendicularly magnetized tunnel junctions, *Phys. Rev. B* **93**, 024420 (2016).
- [75] S. Mizukami, E. P. Sajitha, D. Watanabe, F. Wu, T. Miyazaki, H. Naganuma, M. Oogane, and Y. Ando, Gilbert damping in perpendicularly magnetized Pt/Co/Pt films investigated by all-optical pump-probe technique, *Appl. Phys. Lett.* **96**, 152502 (2010).
- [76] H. Zhang, D. Zhu, W. Kang, Y. Zhang, and W. Zhao, Stochastic Computing Implemented by Skyrmionic Logic Devices, *Phys. Rev. Appl.* **13**, 054049 (2020).
- [77] Takaaki Dohi, Samik DuttaGupta, Shunsuke Fukami, and Hideo Ohno, Formation and current-induced motion of synthetic antiferromagnetic skyrmion bubbles, *Nat. Commun.* **10**, 5153 (2019).
- [78] See-Hun Yang, Kwang-Su Ryu, and Stuart Parkin, Domain-wall velocities of up to  $750 \text{ m s}^{-1}$  driven by exchange-coupling torque in synthetic antiferromagnets, *Nat. Nanotechnol.* **10**, 221 (2015).
- [79] A. A. Thiele, Steady-State Motion of Magnetic Domains, *Phys. Rev. Lett.* **30**, 230 (1973).